



Long-term dynamics of OH* temperatures over central Europe: trends and solar correlations

Christoph Kalicinsky¹, Peter Knieling¹, Ralf Koppmann¹, Dirk Offermann¹, Wolfgang Steinbrecht², and Johannes Wintel¹

¹Institute for Atmospheric and Environmental Research, University of Wuppertal, Wuppertal, Germany

²DWD, Hohenpeissenberg Observatory, Germany

Correspondence to: Christoph Kalicinsky (kalicins@uni-wuppertal.de)

Received: 6 April 2016 – Published in Atmos. Chem. Phys. Discuss.: 7 June 2016

Revised: 26 October 2016 – Accepted: 27 October 2016 – Published: 6 December 2016

Abstract. We present the analysis of annual average OH* temperatures in the mesopause region derived from measurements of the Ground-based Infrared P-branch Spectrometer (GRIPS) at Wuppertal (51° N, 7° E) in the time interval 1988 to 2015. The new study uses a temperature time series which is 7 years longer than that used for the latest analysis regarding the long-term dynamics. This additional observation time leads to a change in characterisation of the observed long-term dynamics.

We perform a multiple linear regression using the solar radio flux F10.7 cm (11-year cycle of solar activity) and time to describe the temperature evolution. The analysis leads to a linear trend of $(-0.089 \pm 0.055) \text{ K year}^{-1}$ and a sensitivity to the solar activity of $(4.2 \pm 0.9) \text{ K (100 SFU)}^{-1}$ (r^2 of fit 0.6). However, one linear trend in combination with the 11-year solar cycle is not sufficient to explain all observed long-term dynamics. In fact, we find a clear trend break in the temperature time series in the middle of 2008. Before this break point there is an explicit negative linear trend of $(-0.24 \pm 0.07) \text{ K year}^{-1}$, and after 2008 the linear trend turns positive with a value of $(0.64 \pm 0.33) \text{ K year}^{-1}$. This apparent trend break can also be described using a long periodic oscillation. One possibility is to use the 22-year solar cycle that describes the reversal of the solar magnetic field (Hale cycle). A multiple linear regression using the solar radio flux and the solar polar magnetic field as parameters leads to the regression coefficients $C_{\text{solar}} = (5.0 \pm 0.7) \text{ K (100 SFU)}^{-1}$ and $C_{\text{hale}} = (1.8 \pm 0.5) \text{ K (100 } \mu\text{T)}^{-1}$ ($r^2 = 0.71$). The second way of describing the OH* temperature time series is to use the solar radio flux and an oscillation. A least-square fit leads to a sensitivity to the solar activity of

$(4.1 \pm 0.8) \text{ K (100 SFU)}^{-1}$, a period $P = (24.8 \pm 3.3)$ years, and an amplitude $C_{\text{sin}} = (1.95 \pm 0.44) \text{ K}$ of the oscillation ($r^2 = 0.78$). The most important finding here is that using this description an additional linear trend is no longer needed. Moreover, with the knowledge of this 25-year oscillation the linear trends derived in this and in a former study of the Wuppertal data series can be reproduced by just fitting a line to the corresponding part (time interval) of the oscillation. This actually means that, depending on the analysed time interval, completely different linear trends with respect to magnitude and sign can be observed. This fact is of essential importance for any comparison between different observations and model simulations.

1 Introduction

The mesopause of the Earth is one of the most variable regions in the atmosphere. There are numerous different influences such as the solar radiation and different types of waves (e.g. tides, planetary waves, gravity waves) that affect the temperature in this region. Thus, the temperature undergoes large variations on very different timescales from minutes to years. The largest variation observed in temperature is the variation in 1 year. This seasonal variation is characterised by an annual, a semi-annual, and a ter-annual component (see e.g. Bittner et al., 2000) and shows maximum to minimum temperature differences of up to 60 K throughout the year (see Fig. 1). The second largest temperature variations are caused by different types of waves. The induced temperature fluctuations occur on timescales from days up

to months in the case of planetary waves (e.g. Bittner et al., 2000; Offermann et al., 2009; Perminov et al., 2014) and on the timescale of several minutes in the case of gravity waves (e.g. Offermann et al., 2011; Perminov et al., 2014). Beside these rather short-term fluctuations the temperature in the mesopause region also exhibits long-term variations on a timescale of several years. Although the amplitudes of these long-term variations are much smaller, the long-term change of the mesopause temperatures is, nevertheless, clearly existent and important. Several previous studies showed the existence of an 11-year modulation of the temperature in coincidence with the 11-year cycle of solar activity which is visible in the number of sunspots and the solar radio flux F10.7 cm (for a review of solar influence on mesopause temperature see Beig, 2011a). The reported sensitivities in the middle to high latitudes of the Northern Hemisphere lie between 1 to 6 K (100SFU)⁻¹. Another type of long-term change is linear trends in the analysed time interval. In the mesopause region of the Northern Hemisphere such trends range from about zero up to a cooling of 3 K decade⁻¹ (for a review of mesopause temperature trends see Beig, 2011b). Trend breaks also seem to be possible where the linear trend switches its sign (positive or negative trend) or the magnitude of the trend significantly changes (for an example of the latter case see Offermann et al., 2010). In cases of such changes in trend (e.g. caused due to changes in trend drivers) a piecewise linear trend approach can be used, in which different linear trends are determined for different time intervals (e.g. Lastovicka et al., 2012).

Beside these variations of the mesopause temperature, Höppner and Bittner (2007) found a quasi 22-year modulation of the planetary wave activity which they derived from mesopause temperature measurements. This observed modulation coincides with the reversal of the solar polar magnetic field, the so-called Hale cycle. The solar polar magnetic field reverses every approximately 11 years at about solar maximum, thus the maximum positive and negative values of magnetic field strength occur between two consecutive solar maxima (e.g. Svalgaard et al., 2005). Several studies exist showing a quasi 22-year modulation of different meteorological parameters such as temperature, rainfall, and temperature variability that are in phase with the Hale cycle or the double sunspot cycle (e.g. Willet, 1974; King et al., 1974; King, 1975; Qu et al., 2012), but no physical mechanism is found for these coincidences. The double sunspot cycle is another type of Hale cycle with a period of about 22 years which is phase-shifted compared to the Hale cycle of the solar polar magnetic field. The maxima and minima of the double sunspot cycle occur at maxima of the sunspot number (e.g. King, 1975; Qu et al., 2012). However, a number of possible influences, also showing a 22-year modulation, are named: galactic cosmic rays (GCR), solar irradiation, and solar wind (e.g. White et al., 1997; Zieger and Mursula, 1998; Scafetta and West, 2005; Miyahara et al., 2008; Thomas et al., 2013; Mursula and Zieger, 2001).

Because of this large number of influences and possible interactions the analysis of the temperatures is not easy to interpret, but due to the different timescales of the variations the different types of influences and phenomena can sometimes be distinguished. In this paper we focus on the long-term variations of the mesopause temperature on timescales larger than 10 years. We use OH* temperatures, which have been derived from ground-based measurements of infrared emissions at a station in Wuppertal (Germany), for our analyses.

The paper is structured as follows. In Sect. 2 we describe the instrument and measurement technique and show the OH* temperature observations, Sect. 3 introduces the Lomb–Scargle periodogram and its properties, and in Sect. 4 we analyse the OH* temperatures regarding solar correlations, long-term trends, and long periodic oscillations. A discussion of the obtained results is given in Sect. 5, and we summarise and conclude in Sect. 6.

2 Observations

2.1 Instrument and measurements

Excited hydroxyl (OH*) molecules in the upper mesosphere/mesopause region emit radiation in the visible and near infrared. The emission layer is located at about 87 km height with a layer thickness of approximately 9 km (full width at half maximum) (e.g. Baker and Stair Jr., 1998; Oberheide et al., 2006). The GRIPS-II (Ground-based Infrared P-branch Spectrometer) instrument is a Czerny–Turner spectrometer with a Ge detector cooled by liquid nitrogen. It measures the emissions of the P1(2), P1(3), and P1(4) lines of the OH*(3,1) band in the near infrared (1.524–1.543 μm) (for extensive instrument description see Bittner et al., 2000, 2002). The measurements are taken from Wuppertal (51° N, 7° E) every night with a time resolution of about 2 min. Thus, a continuous data series throughout the year is obtained with data gaps caused by cloudy conditions only. This results in approximately 220 nights of measurements per year (Oberheide et al., 2006; Offermann et al., 2010). The relative intensities of the three lines are used to derive rotational temperatures in the region of the OH* emission layer (see Bittner et al., 2000, and references therein).

At the beginning of 2011 a newly built instrument was operated next to the GRIPS-II instrument. Simultaneous measurements conducted over a few months showed no significant differences between the two instruments. Unfortunately a detector failure stopped the GRIPS-II measurements in mid-2011, but the new instrument was able to continue the time series of nightly OH* temperatures. Unfortunately, the new instrument had several technical problems in the following period which led to larger data gaps in the years 2012 and 2013. Finally, a reconstruction was performed to set up the GRIPS-N instrument, a Czerny–Turner spectrom-

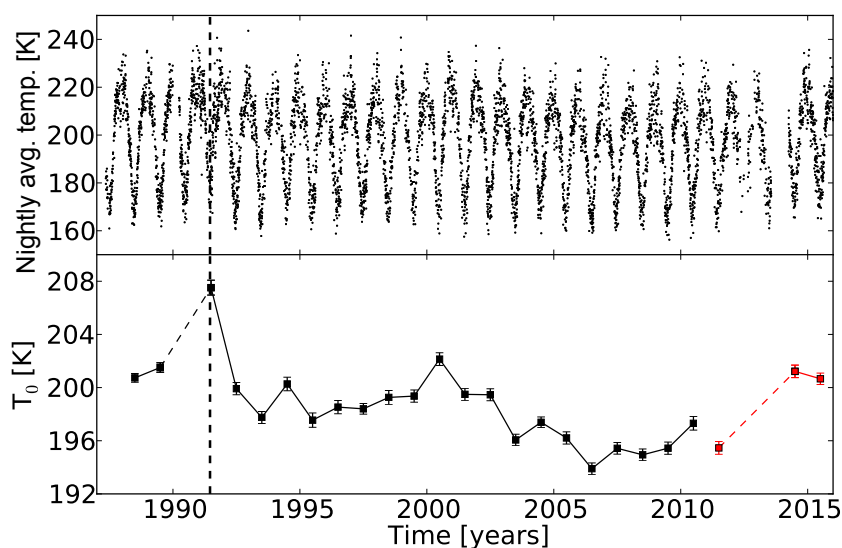


Figure 1. OH* temperature time series derived from GRIPS-II and GRIPS-N measurements at Wuppertal. The upper panel shows the nightly average temperatures and the lower panel shows the annual average temperatures T_0 . Each T_0 is plotted in the middle of the corresponding year and the dates given at the x axis show the beginning of the years. The annual average temperatures partly or completely derived from the new instrument between 2011 and 2015 are shown in red in the lower panel. The error bars show the estimated 1σ uncertainties σ_{T_0} of the temperatures T_0 (based on the standard deviation of the residuals). The vertical dashed line marks the date of Mt Pinatubo eruption.

eter, equipped with a thermoelectrically cooled InGaAs detector. The optical and spectral properties of GRIPS-N and GRIPS-II are very similar, thus the measurements of both instruments are nearly identical. The new GRIPS-N instrument was operated without further problems since the beginning of 2014. Hence, for the years 2014 and 2015 a complete set of measurements is available with only the typical data gaps due to cloudiness.

2.2 Data processing

The nightly average OH* temperatures derived from the GRIPS-II and GRIPS-N measurements in Wuppertal are shown in the upper panel of Fig. 1 for the time interval 1988 to 2015. As mentioned above the data series show larger gaps of several months due to technical problems in the years 2012 and 2013 and, additionally, a data gap of 3 months at the beginning of 1990. These years have to be excluded from the analysis, since a reasonable determination of an annual average temperature in the presence of such large data gaps is not possible.

By far the largest variation in this temperature series is the variation over the course of a year. In order to evaluate the data with respect to long-term dynamics with periods well above 1 year the seasonal variation has to be eliminated first. Since the temperature series exhibits data gaps mostly due to cloudy conditions, a simple arithmetic mean for each year is not advisable. We follow the method used before in several analyses (e.g. Bittner et al., 2002; Offermann et al., 2004, 2006, 2010; Perminov et al., 2014) and perform a harmonic analysis based on least-square fits for each year

separately. As described in Bittner et al. (2000) the seasonal variation is characterised by an annual, a semi-annual, and a ter-annual cycle. Thus, the temperature variation over 1 year is described by

$$T = T_0 + \sum_{i=1}^3 A_i \cdot \sin\left(\frac{2 \cdot \pi \cdot i}{365.25}(t + \phi_i)\right), \quad (1)$$

where T_0 is the annual average temperature, t is the time in days of the year, and A_i , ϕ_i are the amplitudes and phases of the sinusoids. By fitting this equation to the temperature data we can obtain the best possible estimate of the annual average temperature T_0 for each year. A year in this case denotes a calendar year. The resulting annual average temperatures are shown in the lower panel of Fig. 1 with data gaps in the years 1990, 2012, and 2013 (illustrated by the dashed lines). The seasonal variation of the year 2009 is shown in Fig. 2 as a typical example. As described above a detector failure in mid-2011 stopped the GRIPS-II measurements. The following measurements were performed with a new instrument. The first year of full data coverage with GRIPS-N was 2014. Due to this the corresponding T_0 for 2011 and 2014–2015 are marked in red in Fig. 1.

2.3 Comparison with other observations

Since there is a data gap of two years (2012–2013) in the GRIPS-II and GRIPS-N measurements in Wuppertal and the last data points are derived from measurements by a new instrument, one has to ensure that the T_0 from 2011 to 2015 fits the whole picture of long-term temperature evolution.

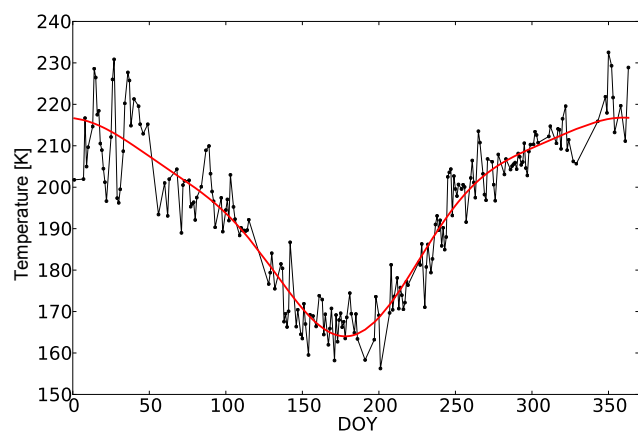


Figure 2. GRIPS-II nightly average temperatures of 2009 plotted at the day of year (DOY). The measurement data are shown in black and the harmonic fit using Eq. (1) is shown as the red curve.

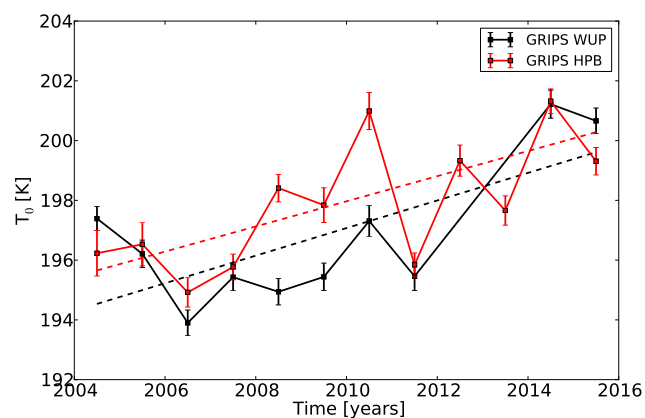


Figure 3. OH* annual average temperatures for the two stations Wuppertal and Hohenpeissenberg in the time interval 2004–2015. The temperatures for Wuppertal (WUP) are shown in black and the temperatures for Hohenpeissenberg (HPB) in red. The dashed lines show the linear fits to the corresponding time series. The linear fit for the Hohenpeissenberg time series only considers measurements at times Wuppertal measurements are also available.

We compare the Wuppertal observations with observations of OH* temperatures taken from Hohenpeissenberg (48° N, 11° E) to check this. The instrument GRIPS-I in Hohenpeissenberg measures in the same spectral range and uses the same data processing technique to determine OH* temperatures. GRIPS-I is an Ebert–Fastie spectrometer with a liquid-nitrogen-cooled Ge detector (see e.g. Bittner et al., 2002). The measurements at Hohenpeissenberg started end of 2003.

Figure 3 shows the comparison for the two measurement stations. A significant correlation between the two time series can be found with a correlation coefficient $r = 0.72$. The comparably low value of r is caused by the differences between 2007 to 2009, where the temperatures at Wuppertal partly decrease (increase) and the Hohenpeissenberg tem-

peratures increase (decrease) at the same time. These differences are most likely caused by local effects. Furthermore, the largest absolute difference in 2010 is caused by an exceptional warm summer observed at Hohenpeissenberg. This warm summer is also observed at the nearby station in Oberpfaffenhofen (see Schmidt et al., 2013, their Fig. 12.) but not at Wuppertal.

The linear increase for each time series is shown in Fig. 3 as dashed lines in black and red. In order to get the most appropriate comparison the linear fit to the Hohenpeissenberg time series only considers data points at times where measurements at Wuppertal are also available. The linear increase during the last 12 years at Wuppertal is $(0.46 \pm 0.17) \text{ K year}^{-1}$ and the increase at Hohenpeissenberg is $(0.42 \pm 0.16) \text{ K year}^{-1}$. Both values agree very well, but the two lines are shifted towards each other indicating an offset between the two stations. This offset is about 0.9 K with Hohenpeissenberg being warmer. In a former study Offermann et al. (2010) obtained a mean offset between the two stations of 0.8 K for the time interval 2004–2008. Thus, this comparison agrees well the former study. Offermann et al. (2010) suggested that the latitudinal difference between the stations is responsible for this small difference. The temperature differences between the minima in 2006 and the maxima in 2014 also agree very well for both stations. The values are $(7.3 \pm 0.7) \text{ K}$ at Wuppertal and $(6.4 \pm 0.7) \text{ K}$ at Hohenpeissenberg. Since we analysed the relative evolution of the temperature series at Wuppertal, the last data points were found to fit the whole picture of the long-term development of OH* temperatures. Thus, the temperature increase observed at Wuppertal in recent years is reliable and confirmed by the temperature increase observed at Hohenpeissenberg.

The latest analysis of the OH* temperatures at Wuppertal regarding long-term dynamics was performed for the time interval 1988–2008 (Offermann et al., 2010). The current study now considers a time series which is 7 years longer than that used before. The clear temperature increase over the last years has encouraged us to perform a new analysis regarding the long-term dynamics.

3 Lomb–Scargle periodogram and false alarm probability

Analysing periodicities in the time series of T_0 using the common fast Fourier transform (FFT) or wavelet analysis is not possible, since the time series exhibits data gaps and these methods rely on equidistant data. A frequently used method in such a situation is the Lomb–Scargle periodogram (LSP), which can handle time series with uneven spacing. The periodogram was developed by Lomb (1976) and Scargle (1982) and is equivalent to the fitting of sinusoids (Horne et al., 1986). It can be calculated for every frequency f , which is another advantage compared to the discrete FFT, which is evaluated at discrete frequencies only. We use the

algorithm by Townsend (2010) for the fast calculation of the periodogram.

An important quantity for the interpretation of a LSP is the so called false alarm probability (FAP). The FAP gives the probability that a peak of height z in the periodogram is caused just by chance, e.g. by noise. As already pointed out by Scargle (1982), the cumulative distribution function (CDF) can be used to determine the FAP. If we take different samples of noise, calculate the LSP for each sample and then determine the height z of the maximum peak, the CDF of all these heights z gives the probability that there is a height Z smaller or equal to z . Consequently, the value $1 - \text{CDF}$ gives the probability that there is a height Z larger than z by chance. Thus, $1 - \text{CDF}$ gives the FAP. Another important point in this context is the normalisation of the periodogram, since the normalisation affects the type of distribution of the periodogram, thus the description of the FAP (for a more detailed discussion see e.g. Horne et al., 1986; Schwarzenberg-Czerny, 1998; Cumming et al., 1999; Zechmeister and Kürster, 2009). We use the normalisation by the total variance of the data, which leads to a beta distribution in the case of Gaussian noise (Schwarzenberg-Czerny, 1998). Since a mean has to be subtracted from the data before calculating the LSP, the total variance is determined using $N - 1$ degrees of freedom with N being the number of data points. This leads to a maximum value for a peak in the periodogram of $(N - 1)/2$ in the case of a single sinusoid. The FAP can be described by

$$\text{FAP} = 1 - \left[1 - \left(\frac{2z}{N - 1} \right)^{(N-3)/2} \right]^{N_i}, \quad (2)$$

where N is the number of data points and N_i is the number of independent frequencies (Schwarzenberg-Czerny, 1998; Cumming et al., 1999; Zechmeister and Kürster, 2009). The number of independent frequencies N_i has to be determined using simulations, since it is not possible to easily describe this quantity analytically (Cumming et al., 1999). It depends on several factors, e.g. the number of data points N and the spacing of the data points. Horne et al. (1986) showed the partly large effect of the spacing (randomly or clumps of points) on N_i . Therefore, we perform simulations to determine N_i for the special situation of our observations. We take random values from a Gaussian distribution and the spacing of our observations as input. Then we calculate the LSP for ten thousand such noise samples in the same way as for the real data and determine the height z of the maximum peak for each LSP. Every LSP is evaluated in the frequency range from Nyquist-frequency $f = 1/2 \text{ year}^{-1}$ to $f = 1/T \text{ year}^{-1}$, where T in our case is 35 years, since we want to search for periodicities in range of the time window of the data series of 28 years. Periodicities in this range are surely accompanied with larger uncertainties, but the LSP gives a reasonable overview over the periodicities, even the large ones, included in the time series. The LSP is calculated at $4T_{\text{dur}}\Delta f = 53$

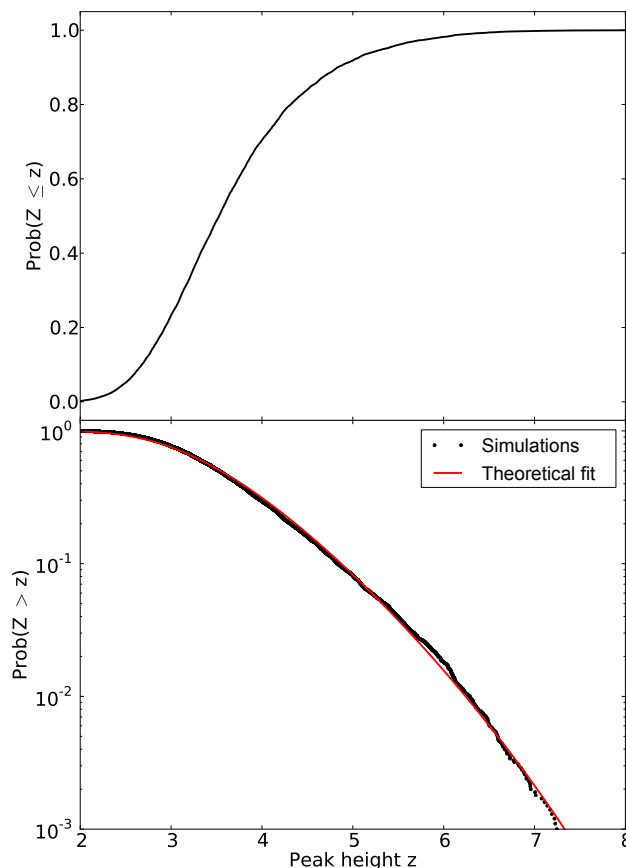


Figure 4. Distribution for peak heights z determined using random values from a Gaussian distribution as input for the calculation of LSP (for details see Sect. 3). The upper panel shows the empirical CDF, thus, the probability that there is a height Z smaller or equal to z . The FAP (probability that a height Z larger z occurs just by chance) is shown in the lower panel. The simulation results are shown in black and a fit to the theoretical curve from Eq. (2) is shown in red. Note the logarithmic scale of the y axis of the lower panel. This calculations are done for a data sampling same as that of the time series from 1988 to 2015 including data gaps. The fit leads to a number of independent frequencies $N_i = 32.4$.

evenly spaced frequencies in the mentioned frequency range, where T_{dur} is the duration of observations. Cumming et al. (1999) pointed out that this is an adequate sampling to observe all possible peaks. The upper panel of Fig. 4 shows the resulting empirical CDF of z for our sampling. The number of data points in this case is $N = 25$ and the data series includes the data gaps in 1990 and 2012–2013. The lower panel of Fig. 4 displays the FAP ($1 - \text{CDF}$) as a black curve. The fit of the theoretical curve using Eq. (2) to this data points is shown in red. The fit leads to a number of independent frequencies $N_i = 32.4$. With knowledge of N_i we can calculate the FAP for every peak height z and determine confidence levels for the LSP.

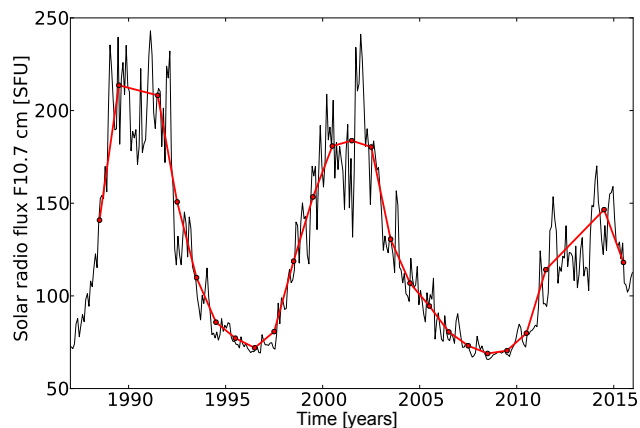


Figure 5. Monthly average values of the solar radio flux F10.7 cm. The red dots mark the annual average values corresponding to the times of the GRIPS data points. The data were provided by Natural Resources Canada, Space Weather Canada.

4 Analysis of long-term dynamics: linear trend, solar correlations, long periodic, and multi-annual oscillations

4.1 Linear trend and 11-year solar cycle

We analyse the long-term trend and the correlation with the 11-year cycle in solar activity by means of a multiple linear regression. For this and the following analyses the time coordinate is shifted such as the first data point (1988.5) is set to zero. The annual average temperatures are described by

$$T_0(t, \text{SF}) = C_{\text{trend}} \cdot t + C_{\text{solar}} \cdot \text{SF} + b, \quad (3)$$

where C_{trend} and C_{solar} are the two regression coefficients, t is the time in years, b is a constant offset, and SF is the solar radio flux F10.7 cm in solar flux units (SFU). The solar radio flux is shown in Fig. 5 for the time interval from 1988 to 2015. The monthly average values of the solar radio flux F10.7 cm were provided by Natural Resources Canada (Space Weather Canada) and were obtained from <http://www.spaceweather.gc.ca/solarflux/sx-5-mavg-en.php>. There are three solar maxima in this time interval at about 1991, 2001, and 2014. This corresponds well to the annual average temperatures T_0 , which also show local maxima at these points. The calculated regression coefficients determined by fitting Eq. (3) using the method of ordinary least squares are $C_{\text{trend}} = (-0.089 \pm 0.055) \text{ K year}^{-1}$ and $C_{\text{solar}} = (4.2 \pm 0.9) \text{ K (100 SFU)}^{-1}$. The p values (for the null hypothesis test) are 0.12 for C_{trend} and below 0.01 for C_{solar} . The 1σ uncertainties for the parameters given here (and in the following cases) are based on the standard deviation of the residuals to account for variations not captured by the fit. The whole fit has a $r^2 = 0.6$. Figure 6 shows the results for this analysis. The upper panel of the figure shows the temperature

time series in black and the fit according to Eq. (3) in red. Additionally, the residual T_{res} is shown in the lower panel. Obviously, a fit taking into account a linear trend and the correlation with the 11-year solar cycle is a relatively poor fit to the temperature time series. When comparing the fit with the temperature time series, one has to additionally keep in mind that the general shape of the fit cannot change, since it depends on the time and solar flux values, which are fixed. The temperature residual still shows a temperature decrease until about 2005 and a temperature increase afterwards. In particular, the large increase at the end of the time series is not captured by the fit. Although there is an increase in solar activity in the same time interval, it is by far not enough to completely explain the observed temperature increase until 2015.

The obvious differences between fit and data series can also be seen in the LSPs in Fig. 7. The LSP is used here to analyse at which periods the determined fit reduces the variance of the original data series. The periodogram for the annual average temperatures T_0 is shown in black and the periodogram for the residual T_{res} after subtracting the fit is shown in red. The LSP for the residual is normalised using the variance of the residual. All variances calculated for residuals in this study are adjusted to account for the reduction of degrees of freedom, which is caused by the subtraction of a fit, using the number of fit parameters. The peak at about 11 years in the LSP for T_0 , which indicates the correlation with the 11-year solar cycle, disappeared after subtracting the fit. In contrast, the large broad peak at the end of the periodogram is not completely removed and the probability that the peak is caused accidentally is only 25%. Since the fit subtracted from the data may contain functions non-orthogonal to the LSP components, which are sinusoids, the remaining peak cannot be interpreted as an oscillation with a period of 20 years that remains or is even a component of the original data series. The peak is likely influenced by the fit subtracted from the data series, e.g. since the subtraction of a linear trend filters out low-frequency components. However, the clear signal in the long periodic range that remains in the periodogram shows that the fit determined by using Eq. (3) is not sufficient to remove all long-term variations. There are two possibilities to describe the long-term variation of the temperature series in a better way. Firstly, one can introduce a trend break so that there is a linear decrease in the first part and a linear increase in the second part of the series. Secondly, one can use a long periodic oscillation, which can introduce a trend break with a smoother transition. We will investigate these two possibilities in the next subsections.

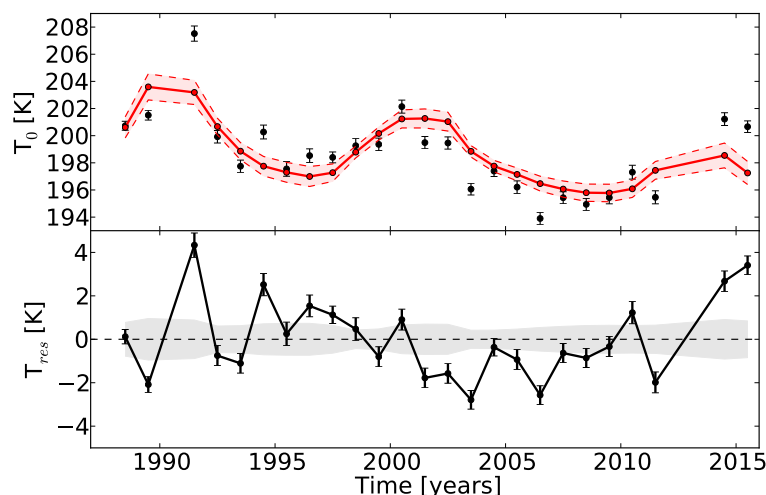


Figure 6. The upper panel of the figure shows the time series of annual average OH* temperatures in black and the fit corresponding to Eq. (3) with the regression coefficients $C_{\text{trend}} = (0.089 \pm 0.055) \text{ K year}^{-1}$ and $C_{\text{solar}} = (4.2 \pm 0.9) \text{ K (100 SFU)}^{-1}$ in red. The black error bars show the uncertainties of the temperatures σ_{T_0} and the reddish area defined by the dashed red lines shows the 1σ uncertainty σ_{fit} of the fit. In the lower panel the residual T_{res} of the two is shown. The black error bars show the uncertainties of the temperatures σ_{T_0} and the gray area around the zero line shows the uncertainty of the fit.

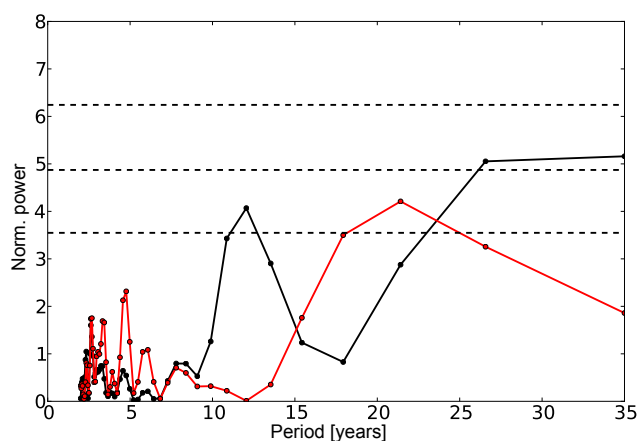


Figure 7. The Lomb–Scargle periodogram for the time series of annual OH* temperatures (see Fig. 1 lower panel) is shown in black and the LPS for the residual after subtracting the fit according to Eq. (3) (see Fig. 6 lower panel) is shown in red. The LSP is evaluated at 53 evenly spaced frequencies in the range $f = 1/2 \text{ year}^{-1}$ to $f = 1/35 \text{ year}^{-1}$. The dashed black horizontal lines display the levels for false alarm probabilities of 0.01, 0.1, and 0.5 (top to bottom). The false alarm probabilities are calculated according to Eq. (2) using $N_i = 32.4$ and the number of data points $N = 25$.

4.2 Trend break

The trend break and the correlation with the 11-year solar cycle are analysed by describing the annual average temperatures as

$$T_0(t, \text{SF}) = C_{\text{solar}} \cdot \text{SF} + \text{trend}_{2\text{phase}}(t), \quad (4)$$

where $\text{trend}_{2\text{phase}}(t)$ is a trend term using two lines to introduce the trend break. The trend term is written as

$$\text{trend}_{2\text{phase}}(t) = \begin{cases} C_{\text{trend1}} \cdot t + b_1 & : t \leq \text{BP} \\ C_{\text{trend2}} \cdot t + b_2 & : t > \text{BP} \end{cases}, \quad (5)$$

where BP is the break point (in years). Since the two different lines need to be equal at the break point, this leads to the condition

$$\begin{aligned} C_{\text{trend1}} \cdot \text{BP} + b_1 &= C_{\text{trend2}} \cdot \text{BP} + b_2 \\ \Leftrightarrow b_2 &= b_1 + (C_{\text{trend1}} - C_{\text{trend2}}) \cdot \text{BP}. \end{aligned} \quad (6)$$

Thus, Eq. (5) can be rewritten as

$$\begin{aligned} \text{trend}_{2\text{phase}}(t) &= \begin{cases} C_{\text{trend1}} \cdot t + b_1 & : t \leq \text{BP} \\ C_{\text{trend2}} \cdot t + (b_1 + (C_{\text{trend1}} - C_{\text{trend2}}) \cdot \text{BP}) & : t > \text{BP} \end{cases} \end{aligned} \quad (7)$$

The description of the concept and the condition can be seen in Ryan and Porth (2007). Equation (4) now describes the annual average temperatures by using the correlation with the solar flux and a trend term with two different phases, where both phases have a linear temperature behaviour. These two phases are coupled by the variable break point BP.

We determine the best estimates for the parameters C_{solar} , C_{trend1} , C_{trend2} , b_1 , and BP by means of a least-square fit. The fit leads to a sensitivity to the solar flux of $C_{\text{solar}} = (3.3 \pm 0.9) \text{ K (100 SFU)}^{-1}$. After subtracting this solar dependence and the mean, the resulting residual, and the best fit of the trend term are shown in Fig. 8 as black and red lines respectively. Additionally, the position of the break point and the corresponding uncertainties are marked as a vertical black line and vertical dashed black lines respectively. We observe a trend

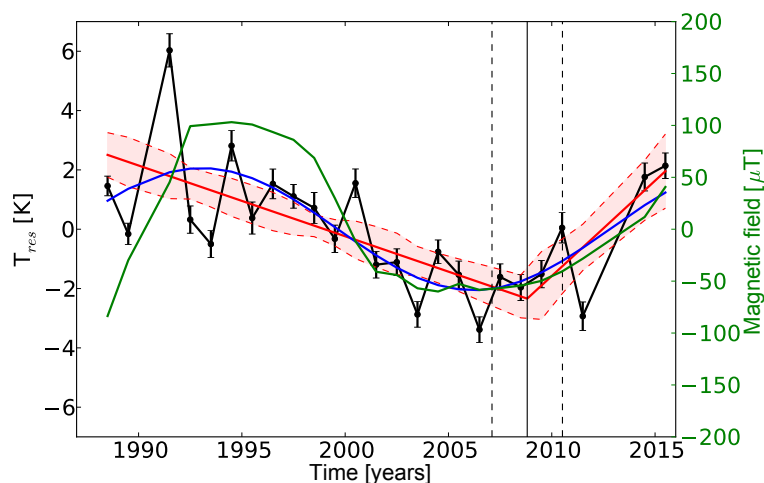


Figure 8. Residual for the temperature time series after removing the 11-year solar cycle ($C_{\text{solar}} = (3.3 \pm 0.9) \text{ K } (100 \text{ SFU})^{-1}$) and subtracting the mean. The black error bars show the uncertainties σ_{T_0} . The red lines show the fit according to Eq. (7) and the blue curve the fit according to Eq. (8). The reddish area defined by the red dashed lines shows the 1σ uncertainty σ_{fit} of the complete fit according to Eq. (7). The break point BP is marked by the vertical black line and the corresponding uncertainties are shown as vertical dashed black lines. Additionally, the annual average values of the solar polar magnetic field strength are displayed as a green curve with a second axis to the right. Shown are the average values for the solar North Pole and South Pole with the magnetic field orientation of the North Pole $((N-S)/2)$. The data were provided by the Wilcox Solar Observatory (for an instrument description see Scherrer et al., 1977).

break in the middle of 2008 ($\text{BP} = (2008.8 \pm 1.7) \text{ year}$). Before the trend break in 2008 there is a negative temperature trend $C_{\text{trend1}} = (-0.24 \pm 0.07) \text{ K year}^{-1}$ and after the break point the trend is positive with a slope $C_{\text{trend2}} = (0.64 \pm 0.33) \text{ K year}^{-1}$. The r^2 of the whole fit is 0.74. The LSP for the residual after subtracting the trend break fit is shown in Fig. 9 in red. The former large peak at the right end of the periodogram for the original data series (black curve) is nearly completely removed after subtracting the trend break fit. Thus, the fit using two linear trends and a trend break explains a very large portion of the long-term variation of the OH* temperature series.

4.3 Long-term oscillation

We analyse the possibility of an oscillation instead of a trend break. In order to get an idea about the oscillation we fit a sinusoid of the form

$$T_{\text{res}}(t) = A \cdot \sin\left(\frac{2 \cdot \pi}{P}(t + \phi)\right) + b \quad (8)$$

to the temperature residual after subtracting the solar dependence and the mean (see Fig. 8 black curve). A denotes the amplitude, P the period, and ϕ the phase. Additionally, we fit an offset b , since the mean of the temperature residual is not necessarily identical to the zero crossing of the oscillation. The resulting oscillation is shown in Fig. 8 as a blue curve. The important estimated parameters of the fit are an amplitude $A = (2.06 \pm 0.43) \text{ K}$ and a period of about 26 years ($P = (26.3 \pm 3.2) \text{ years}$). It is clear that this oscillation and the fit using the two linear phases and a trend break

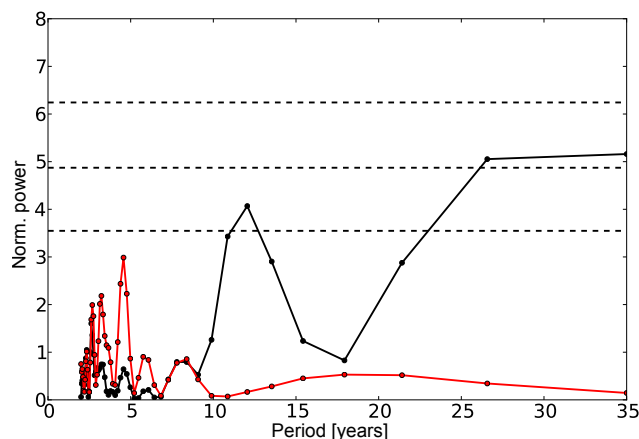


Figure 9. The Lomb–Scargle periodogram for the time series of annual OH* temperatures (see Fig. 1 lower panel) is shown in black and the LPS for the residual after subtracting the fit according to Eq. (4) is shown in red. For details see description of Fig. 7.

(red lines in Fig. 8) are nearly identical for the time interval after 2008. Before 2008 the blue curve oscillates about the red line. Additionally, the oscillation introduces a much smoother transition from decreasing to increasing temperatures. The decrease in variance is larger for the oscillation than for the fit using two linear phases. The variances of the two resulting differences, T_{res} minus linear trends (red lines) and oscillation (blue curve) are 2.64 and 2.44 K^2 . Offermann et al. (2010) already suggested a trend break in the temperature series at about 1997. The oscillation would account for

such a second trend break in the temperature series in the mid-1990s, about 1993.

Very prominent is the fact that the oscillation has a period of about 26 years with a minimum at about 2006 and a maximum at about 1993. This type of oscillation with very similar parameters can be found on the sun. The original solar cycle (Hale cycle) is a cycle with a period of about 22 years and describes the reversal of the magnetic field of the sun. The solar polar magnetic field of the sun is shown in Fig. 8 as a green curve with a second axis to the right. The solar polar field strength data were provided by the Wilcox Solar Observatory and were obtained from <http://wso.stanford.edu/Polar.html>. We used the low pass filtered values. Evidently, the oscillation fitted to T_{res} and the Hale cycle of the magnetic field are very similar in the time interval shown. The correlation coefficient for a linear regression between the magnetic field and the temperature residual (black curve in Fig. 8) is $r = 0.55$. The corresponding slope is $(1.74 \pm 0.56) \text{ K } (100 \mu\text{T})^{-1}$ (p value < 0.01). This is a remarkable accordance between the observed oscillation in atmospheric temperature and solar polar magnetic field.

The long periodic oscillation describes the largest part of the temperature variability after detrending the temperature series with respect to the 11-year solar cycle. Thus, we analyse the temperature series T_0 by means of a multiple linear regression again to fit all dependencies simultaneously. We include the solar polar magnetic field in the equation, which replaces the linear trend. Hence, Eq. (3) transforms to

$$T_0(\text{SF}, B_{\text{solar}}) = C_{\text{solar}} \cdot \text{SF} + C_{\text{hale}} \cdot B_{\text{solar}} + b, \quad (9)$$

where B_{solar} denotes the solar polar magnetic field and C_{hale} the corresponding regression coefficient. The analysis leads to the results for the regression coefficients $C_{\text{solar}} = (5.0 \pm 0.7) \text{ K } (100 \text{ SFU})^{-1}$ and $C_{\text{hale}} = (1.8 \pm 0.5) \text{ K } (100 \mu\text{T})^{-1}$. The fit to the temperature time series has a $r^2 = 0.71$. This value is larger than the value for the fit including the 11-year solar cycle and one linear trend, which has a $r^2 = 0.6$ (see Sect. 4.1), but it is slightly lower than the $r^2 = 0.74$ of the trend break fit (see Sect. 4.2). An additional linear trend added to Eq. (9) does not significantly change the results. The obtained linear trend is insignificant in this case; therefore, it is excluded. The resulting fit and the residual are shown in Fig. 10. The fit curve (red colour) shows good agreement with the long-term variation of the temperature (black dots), but there are still some differences, especially at the beginning and the end of the time series. Additionally, the temperature residual (lower panel of Fig. 10) seems to show a long periodic oscillation. The LSP for the residual (red curve in Fig. 11) shows that the former large peak at the long periodic end of the periodogram (black curve) is largely reduced after subtracting the fit, which shows that the description using the 11-year solar cycle and the Hale cycle explains most of the variance in the long periodic range. It is possible that an oscillation with similar parameters to the Hale cycle, which

are slightly changed (in amplitude, phase, and/or period), can describe the annual average temperatures even better.

We analyse this possibility and add an oscillation to the temperature description, which replaces the solar polar magnetic field. Since the oscillation and the 11-year solar cycle are non-orthogonal functions, here we fit all dependencies simultaneously. The equation transforms to

$$T_0(\text{SF}, t) = C_{\text{solar}} \cdot \text{SF} + C_{\text{sin}} \cdot \sin\left(\frac{2 \cdot \pi}{P}(t + \phi)\right) + b, \quad (10)$$

where C_{sin} is the amplitude, P is the period, ϕ is the phase of the oscillation, and t is the time in years. The results of the least-square fit are $C_{\text{solar}} = (4.1 \pm 0.8) \text{ K } (100 \text{ SFU})^{-1}$ for the sensitivity to the solar activity, $C_{\text{sin}} = (1.95 \pm 0.44) \text{ K}$ for the amplitude, and $P = (24.8 \pm 3.3) \text{ years}$ for the period of the oscillation. The obtained oscillation is hereafter denoted “the 25-year oscillation”. The fit has a $r^2 = 0.78$. Compared to the trend break fit (see Sect. 4.2) the increase in r^2 is not significant, thus both descriptions are likely and lead to equivalent results. The fit and the residual are shown in Fig. 12. The temperature residual (lower panel of Fig. 12) no longer shows obvious long-term variations; neither a linear trend nor an oscillation. Only some variations with periods of the order of several years remain. The LSP for the temperature residual, which is shown in Fig. 13, confirms this. All long-term variations with periods larger than about 10 years are now removed from the temperature series. There are only peaks in the range up to a period of about 8 years. Thus, the description of the annual average temperature including the 11-year solar cycle and an oscillation with a period of 25 years is sufficient to explain all long-term variations. No further linear trend can be found in the data series.

4.4 Stability of solar sensitivity

In the former sections a constant sensitivity to the solar activity for the complete observations was assumed. In order to study whether this assumption is correct and the oscillation derived in Sect. 4.3 is still obtained if the solar sensitivity is allowed to vary, we analyse the time series of annual temperatures again. For the analysis we use time intervals of 11 years (approximately the length of one solar cycle). We start with the interval 1988–1998 and always shift the time interval by 1 year, ending with the interval 2005–2015. Time intervals that do not cover a 11-year window because of missing data at the end or beginning of the interval are excluded from the analysis. All possible time intervals are analysed separately. The temperatures in each interval are described by Eq. (3) and the coefficients C_{trend} and C_{solar} are determined. By doing this, we assume a linear trend in each time interval, but the trend and the sensitivity to the solar activity are allowed to vary from one interval to the next.

The results of the analysis are shown in Fig. 14. The sensitivity to the solar activity is shown in the upper panel of the figure in black, and the grey shaded area marks the range

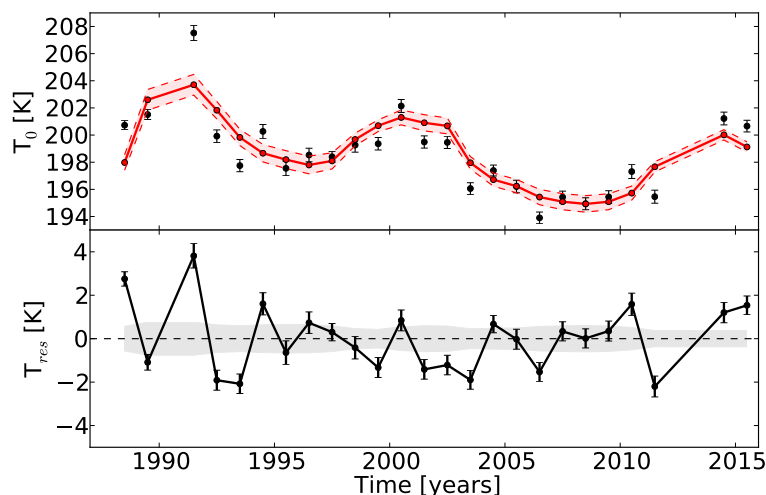


Figure 10. The upper panel of the figure shows the time series of annual average OH* temperatures in black and the fit corresponding to Eq. (9) with the regression coefficients $C_{\text{hale}} = (1.8 \pm 0.5) \text{ K } (100 \mu\text{T})^{-1}$ and $C_{\text{solar}} = (5.0 \pm 0.7) \text{ K } (100 \text{ SFU})^{-1}$ in red. In the lower panel the residual T_{res} of the two is shown. For description of displayed uncertainties see Fig. 6.

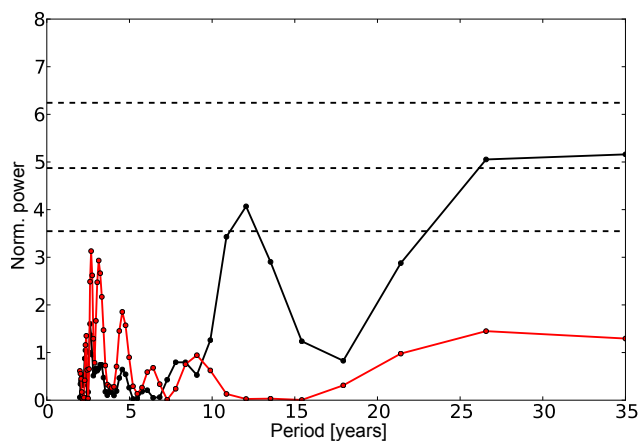


Figure 11. The Lomb–Scargle periodogram for the time series of annual OH* temperatures (see Fig. 1 lower panel) is shown in black and the LPS for the residual after subtracting the fit according to Eq. (9) (see Fig. 10 lower panel) is shown in red. For details see description of Fig. 7.

for the sensitivity derived in Sect. 4.3 for the fit using the solar cycle and an oscillation $((4.1 \pm 0.8) \text{ K } (100 \text{ SFU})^{-1})$. The sensitivities derived for the 11-year time intervals show some variations but considering the uncertainties no significant changes can be observed. The mean of the derived sensitivities is $(3.9 \pm 0.3) \text{ K } (100 \text{ SFU})^{-1}$, which agrees very well with the value derived before.

The lower panel of Fig. 14 shows the derived linear trends in black. We fit a sinusoid to these trend values (red line in figure) that results in the values $A = (0.36 \pm 0.06) \text{ K}$ for the amplitude and $P = (23.2 \pm 2.5) \text{ years}$ for the period. This oscillation found in the trend values should be equal to the

derivative of the 25-year oscillation derived in Sect. 4.3 with a reduced amplitude, since 11-year time intervals are used, so no local derivative is obtained. This agreement is indeed the case. The observed period of the trend oscillation agrees within the uncertainties with the 25-year oscillation derived in the former section and the phase is also correct. The 25-year oscillation of the temperature is shown in the lower panel of Fig. 14 in blue and the corresponding derivative in green (with a second axis to the right). It appears that the green and red curve are nearly identical. In total the analysis method using 11-year time intervals leads to the same results as the fit including the sensitivity to the solar cycle and an oscillation to the whole data series. So this analysis confirms the results obtained in Sect. 4.3.

5 Discussion

5.1 11-year solar cycle

There are numerous publications about the correlation of the 11-year cycle of solar activity and temperatures in the mesopause region. A review is given by Beig (2011a, see Fig. 2 and corresponding section). The sensitivity to the solar activity in the northern middle to high latitudes reported in this review is about 1–6 K $(100 \text{ SFU})^{-1}$. In a more recent study on mesopause temperatures measured at Zvenigorod (56° N , 37° E ; 2000–2012) by Perminov et al. (2014) a sensitivity of $(3.5 \pm 0.8) \text{ K } (100 \text{ SFU})^{-1}$ is found. This value perfectly agrees with the result of a former analysis of the GRIPS measurements at Wuppertal (1988–2008), where a sensitivity of $(3.5 \pm 0.2) \text{ K } (100 \text{ SFU})^{-1}$ was also found (Offermann et al., 2010). In our study we obtained results in the range 3–5 K $(100 \text{ SFU})^{-1}$. Depending on the analysis

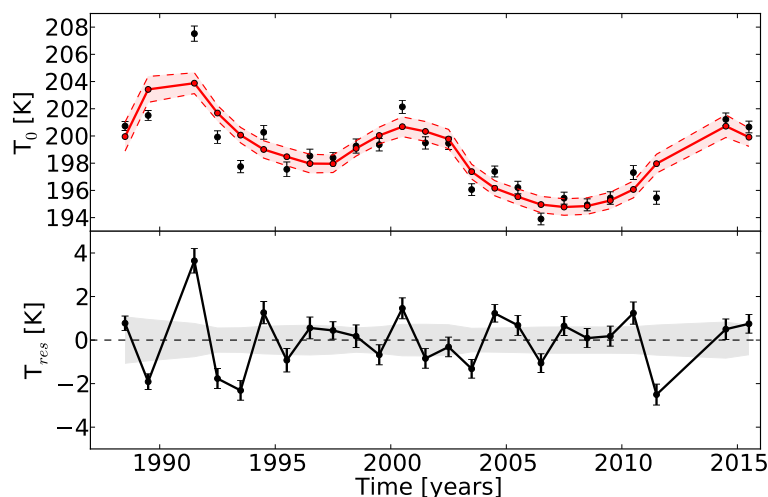


Figure 12. The upper panel of the figure shows the time series of annual average OH* temperatures in black and the fit corresponding to Eq. (10) with the coefficients $C_{\text{solar}} = (4.1 \pm 0.8) \text{ K (100SFU)}^{-1}$, $C_{\text{sin}} = (1.95 \pm 0.44) \text{ K}$, and $P = (24.8 \pm 2.1) \text{ years}$ in red. In the lower panel the residual T_{res} of the two is shown. For description of displayed uncertainties see Fig. 6

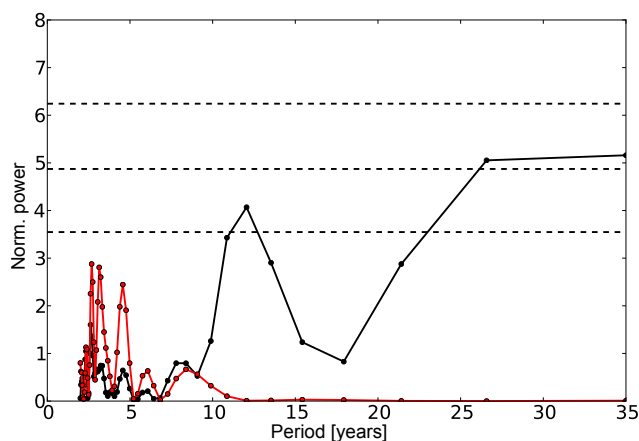


Figure 13. The Lomb–Scargle periodogram for the time series of annual OH* temperatures (see Fig. 1 lower panel) is shown in black and the LPS for the residual after subtracting the fit according to Eq. (10) (see Fig. 12 lower panel) is shown in red. For details see description of Fig. 7.

method the results differ slightly from each other, but they nearly all agree within the uncertainties (only the value derived by using the Hale cycle seems to be a little too large). Since the parameters for the fits (solar radio flux, solar polar magnetic field, oscillation, and time) are not completely independent of each other, the derived coefficients are only approximations of the true values. A much longer time series, including more solar maxima, would be necessary to finally derive the true coefficients. Thus, small differences in the derived values are expected, especially in the case of the multiple linear regression including the solar radio flux and the linear trend, since this regression leads to a result

that cannot completely explain all long-term trends and oscillations in the time series. Nearly all derived values for the sensitivity of the OH* temperatures to the 11-year solar cycle are slightly larger than the one derived in the former analysis of the GRIPS measurements at Wuppertal. However, the time intervals are different for the analyses, which can lead to different results for the derived sensitivities. This aspect was already discussed by Offermann et al. (2010).

Besides the fact that the derived values are in the expected range for the northern middle to high latitudes, one new aspect with respect to the correlation between 11-year solar cycle and mesopause temperatures has become apparent. In the present study the correlation was determined for three solar maxima including the comparably weak latest solar cycle 24. Our study shows that the significant correlation between OH* temperatures and the 11-year solar cycle is still evident in this case.

5.2 Linear trend and trend break

Temperature trends in the mesopause region are reported in a number of papers, and a review about numerous results is given by Beig (2011b, see Fig. 2 and corresponding section). The temperature trends reported there range between no trend up to a cooling of about 3 K decade^{-1} . Recent studies by different authors lead to the following results. Combined Na lidar observations at Fort Collins (41° N , 105° W) and Logan (42° N , 112° W) in the time interval 1990–2014 lead to an insignificant trend of $(-0.64 \pm 0.99) \text{ K decade}^{-1}$ at 85 km and the negative trend increases with increasing height up to a maximum of $(-2.8 \pm 0.58) \text{ K decade}^{-1}$ at 91 and 93 km (She et al., 2015). The analysis by Perminov et al. (2014) for the measurements at Zvenigorod (56° N , 37° E) showed a trend of $(-2.2 \pm 0.9) \text{ K decade}^{-1}$

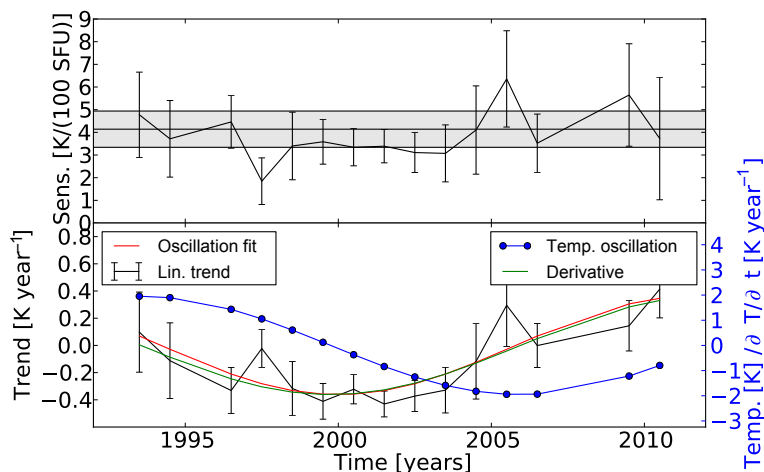


Figure 14. The upper panel shows the sensitivity to the solar activity derived for different 11-year time intervals. All values are displayed at the middle of the corresponding time interval. The error bars show the 1σ uncertainties. The grey shaded area marks the range of the sensitivity derived in Sect. 4.3 for the fit using the solar cycle and one oscillation ($C_{\text{solar}} = (4.1 \pm 0.8) \text{ K (100SFU)}^{-1}$). The lower panel of the figure shows the corresponding linear trends for each time interval in black. A sinusoid fitted to these values is shown in red. The result for the 25-year temperature oscillation (see Sect. 4.3) is shown as a blue curve and the corresponding derivative of the oscillation is shown as a green curve with a second axis to the right.

for the time interval 2000–2012. Hall et al. (2012) derived a trend of $(-4 \pm 2) \text{ K decade}^{-1}$ from meteor radar observations over Svalbard (78° N , 16° E) at 90 km for the time interval 2001–2012. In a former study of the Wuppertal OH* temperature series (1988–2008) a negative trend of $(-2.3 \pm 0.6) \text{ K decade}^{-1}$ was found (Offermann et al., 2010). The multiple linear regression using the solar radio flux and time as parameters in this paper results in a cooling trend of $(-0.89 \pm 0.55) \text{ K decade}^{-1}$ for the Wuppertal OH* temperatures from 1988 to 2015 (see Sect. 4.1), which is in good agreement with the observations by She et al. (2015). The value is smaller than the trend derived in the former study of the Wuppertal data. Since there has been an increase in temperature from about 2006, and the former study by Offermann et al. (2010) ended in 2008, this temperature increase leads to a smaller negative trend in our study. However, as shown above, one linear trend is not sufficient to account for all long-term variation in the time series. Due to this we introduced a trend break and found a negative trend before 2008 and a positive trend afterwards. The obtained values are $(-2.4 \pm 0.7) \text{ K decade}^{-1}$ and $(6.4 \pm 3.3) \text{ K decade}^{-1}$ (see Sect. 4.2). The time interval used in the former study of the Wuppertal OH* temperature series by Offermann et al. (2010) is nearly identical to the time interval of the first phase, showing the negative temperature trend. The linear temperature trends derived by Offermann et al. (2010) and in this study perfectly agree for this time interval. Due to the additional 7 years of observations this study now clearly shows that the former negative linear trend turned into a positive trend in the last years. This finding is contrary to the other recent studies (She et al., 2015; Perminov et al., 2014; Hall

et al., 2012; Mokhov and Semenov, 2014), where no trend break in the mid-2000s is reported.

5.3 Long-term oscillation

The observed trend break can also be described using a long periodic oscillation. In Sect. 4.3 we show two different possibilities for such a long periodic oscillation.

Firstly, the solar polar magnetic field (Hale cycle) is used as one parameter in a multiple linear regression with the second parameter being the solar radio flux. The correlation coefficients are $C_{\text{solar}} = (5.0 \pm 0.7) \text{ K (100SFU)}^{-1}$ and $C_{\text{hale}} = (1.8 \pm 0.5) \text{ K (100}\mu\text{T)}^{-1}$ ($r^2 = 0.71$). Especially at the beginning and the end of the time series the fit curve does not perfectly match the observations (see Fig. 10). Additionally, the LSP for the temperature residual after subtracting this fit curve still shows a peak in the long periodic range (red curve in Fig. 11), although this is not significant. Thus, the Hale cycle together with the 11-year solar cycle might not explain all observed long-term dynamics. Because of these facts, we believe that the solar polar magnetic field acting as an input parameter is not very suitable.

Secondly, an independent oscillation is used to describe the OH* temperature time series. A least-square fit using the solar radio flux and an oscillation with free amplitude, period, and phase leads to the coefficients $C_{\text{solar}} = (4.1 \pm 0.8) \text{ K (100SFU)}^{-1}$, $C_{\text{sin}} = (1.95 \pm 0.44) \text{ K}$ for the amplitude, and $P = (24.8 \pm 3.3) \text{ years}$ for the period. ($r^2 = 0.78$). After subtracting the derived fit curve the LSP for the residual does not show any remaining long periodic signals (see Fig. 13). The obtained 25-year oscillation, shown in Fig. 15 as a black curve with full circles, is phase-

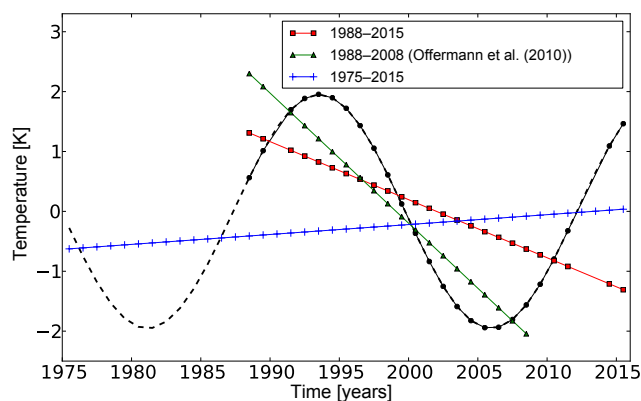


Figure 15. 25-year oscillation of OH* temperatures resulting from the least-square fit using Eq. (10). The coefficients are $C_{\sin} = (1.95 \pm 0.44)$ K, and $P = (24.8 \pm 2.1)$ years. The solid black line with full circles shows the oscillation for the analysed time interval 1988–2015 and the dashed black line shows the continuation of this oscillation back to 1975. The red line with squares displays a linear fit to the oscillation for the time interval 1988–2015, the green line with triangles the fit for the interval 1988–2008, and the blue line with plus signs a fit to the interval 1975–2015.

shifted compared to the Hale cycle and the extrema occur slightly before the extrema of the solar polar magnetic field (compare green curve in Fig. 8 and black curve in Fig. 15, e.g. maximum at about 1993 compared to 1994/1995). This time shift supports the opinion that the Hale cycle is not very likely as an acting input parameter. The nature of the 25-year oscillation is not clear yet, but a self-sustained oscillation in the atmosphere would be a real possibility. Such oscillations were recently discovered by Offermann et al. (2015). An oscillation with a period of about 20 to 25 years is found in various atmospheric parameters such as temperature (Qu et al., 2012; Wei et al., 2015), geopotential height (Coughlin and Tung, 2004a, b), and planetary wave activity (Jarvis, 2006; Höppner and Bittner, 2007). It is also seen in two atmospheric models (HAMMONIA, WACCM). A detailed discussion is, however, beyond the scope of this paper.

The most important point here is that no additional linear trend can be maintained. All long-term dynamics of the Wuppertal OH* temperature time series can be described as a combination of the 11-year solar cycle and a 25-year oscillation. With the knowledge of this 25-year oscillation the linear trends derived in this study (see Sect. 4.1) and a former study of the Wuppertal OH* temperature time series can be reproduced. Figure 15 demonstrates that very different trends can be obtained if specific time intervals of the (sinusoidal) data are used. By fitting a line to the corresponding part (time interval) of the data we obtain the linear trend. The linear trend for the time interval analysed in this study (1988–2015) is (-0.097 ± 0.032) K year⁻¹, which is the same as the linear trend $C_{\text{trend}} = (-0.089 \pm 0.055)$ K year⁻¹ derived by using a multiple linear regression with time and solar radio flux

as parameters (see Sect. 4.1). This linear trend is shown in Fig. 15 as a red line with squares. Offermann et al. (2010) derived a linear trend for the time interval 1988–2008 of (-0.23 ± 0.06) K year⁻¹. A linear fit to the data for this time interval leads to a slope of (-0.22 ± 0.03) K year⁻¹ (green line with triangles in Fig. 15). Thus, the 25-year oscillation “explains” the derived linear trends of this and the former study as well as the obvious trend break observed in the data series. This means that all different kinds of linear trends are possible depending on the time interval which is analysed. If we continue the oscillation back to 1975 (black dashed line in Fig. 15) and fit a line to these data for the whole time interval (1975–2015; blue line with plus signs) in Fig. 15, this leads to a slope of (0.017 ± 0.018) K year⁻¹. This continuation is certainly an assumption and cannot be verified by the observations, but it is likely and clearly shows the possible effects. The presence of such a long periodic oscillation that, in combination with the 11-year solar cycle, explains all long-term dynamics without an additional linear trend is very important with respect to any kind of comparison between different observations or model simulations. Each comparison of linear trends is only valid if the same time interval is analysed. Furthermore, the current study suggests that there is no universal linear trend which is valid for all time intervals at this altitude.

5.4 Stability of solar sensitivity

The analysis by using different 11-year time intervals leads to two main results. Firstly, the sensitivity to the solar activity is fairly stable throughout the whole time period 1988–2015. There are some variations in sensitivity but considering the uncertainties there are no significant changes. The mean of the derived values is (3.9 ± 0.3) K (100 SFU)⁻¹. This value is in nearly perfect agreement with the result of (4.1 ± 0.8) K (100 SFU)⁻¹ for the fit including the 11-year solar cycle and one oscillation using the whole data series at once. So the assumption that the sensitivity to the solar activity is constant during the whole time period is valid for the Wuppertal OH* observations.

Secondly, the derived partial trend values show the same oscillation as the derivative of the 25-year temperature oscillation. Thus, the analysis using the 11-year time intervals confirms the result that, besides the 11-year solar cycle, an oscillation of about 25 years is the second important component of the OH* temperatures observed at Wuppertal.

6 Summary and conclusions

We present the analysis of the OH* temperatures derived from the GRIPS measurements at Wuppertal. We use annual average temperatures in the time interval 1988 to 2015 for our study. The study focuses on the long-term dynamics and leads to the following results.

1. The OH* temperatures show a significant correlation with the solar radio flux. We find a sensitivity to the 11-year solar cycle of $3\text{--}5\text{ K (100SFU)}^{-1}$.
2. One linear trend during the whole time interval (together with the sensitivity to the 11-year solar cycle) cannot sufficiently explain all long-term dynamics found in the OH* temperatures. We introduce a trend break to better account for these long-term dynamics. The best representation of the temperature series is found if the trend break occurs in mid-2008 ($BP = (2008.8 \pm 1.7)\text{ years}$). Before the break point the linear trend is negative and after the break point the trend turns positive with the slopes of $(-0.24 \pm 0.07)\text{ K year}^{-1}$ and $(0.64 \pm 0.33)\text{ K year}^{-1}$.
3. The reversal of the temperature trend can also be described by a long periodic oscillation. We present two possibilities for this oscillation. Firstly, the solar polar magnetic field of the sun (Hale cycle) is used in a multiple linear regression together with the solar radio flux as second parameter. The derived regression coefficients are $C_{\text{solar}} = (5.0 \pm 0.7)\text{ K (100SFU)}^{-1}$ and $C_{\text{hale}} = (1.8 \pm 0.5)\text{ K (100}\mu\text{T)}^{-1}$ ($r^2 = 0.71$). Secondly, an independent oscillation is used instead of the Hale cycle. A least-square fit leads to the coefficients $C_{\text{solar}} = (4.1 \pm 0.8)\text{ K (100SFU)}^{-1}$, $C_{\text{sin}} = (1.95 \pm 0.44)\text{ K}$ for the amplitude, and $P = (24.8 \pm 3.3)\text{ years}$ for the period. The most important point here is that no additional linear trend is needed.
4. Caution has to be applied when estimating linear trends from data sets containing long-term variations. Trend results are quite sensitive to the length of the data interval used. In such a case a piecewise linear trend approach has to be used or the long-term variation has to be described in another appropriate way, e.g. by using an oscillation.

7 Data availability

The GRIPS data used in this study can be obtained by request to the corresponding author or to P. Knieling (knieling@uni-wuppertal.de). The monthly average values of the solar radio flux F10.7 cm were provided by Natural Resources Canada (Space Weather Canada) and were obtained from <http://www.spaceweather.gc.ca/solarflux/sx-5-mavg-en.php>. The solar polar field strength data were provided by the Wilcox Solar Observatory and were obtained from <http://wso.stanford.edu/Polar.html>.

Acknowledgements. This work was funded by the German Federal Ministry of Education and Research (BMBF) within the ROMIC (Role Of the Middle atmosphere In Climate) project MALODY (Middle Atmosphere LOnG period DYnamics) under Grant no. 01LG1207A. Wilcox Solar Observatory data used in this study was obtained via the web site <http://wso.stanford.edu> at 2016:04:11_08:31:21 PDT courtesy of J. T. Hoeksema. The Wilcox Solar Observatory is currently supported by NASA. The solar radio flux 10.7 cm data was obtained from the Natural Resources Canada, Space Weather Canada website: <http://www.spaceweather.gc.ca/>.

Edited by: F.-J. Lübken

Reviewed by: J. Laštovicka and one anonymous referee

References

- Baker, D. J., and Stair Jr., A. T.: Rocket measurements of the altitude distributions of the hydroxyl airglow, *Phys. Scr.*, 37, 611, doi:10.1088/0031-8949/37/4/021, 1998.
- Beig, G.: Long term trends in the temperature of the mesosphere/lower thermosphere region: 2. Solar response, *J. Geophys. Res.*, 116, A00H12, doi:10.1029/2011JA016766, 2011a.
- Beig, G.: Long term trends in the temperature of the mesosphere/lower thermosphere region: 1. Anthropogenic influences, *J. Geophys. Res.*, 116, A00H11, doi:10.1029/2011JA016646, 2011b.
- Bittner, M., Offermann, D., and Graef, H. H.: Mesopause temperature variability above a midlatitude station in Europe, *J. Geophys. Res.*, 105, 2045–2058, doi:10.1029/1999JD900307, 2000.
- Bittner, M., Offermann, D., Graef, H. H., Donner, M., and Hamilton, K.: An 18-year time series of OH* rotational temperatures and middle atmosphere decadal variations, *J. Atmos. Sol. Terr. Phys.*, 64, 1147–1166, doi:10.1016/S1364-6826(02)00065-2, 2002.
- Coughlin, K. and Tung, K. K.: Eleven-year solar cycle signal throughout the lower atmosphere, *J. Geophys. Res.*, 109, D21105, doi:10.1029/2004JD004873, 2004a.
- Coughlin, K. T. and Tung, K. K.: 11-Year solar cycle in the stratosphere extracted by the empirical mode decomposition method, *Adv. Space Res.*, 34, 323–329, doi:10.1016/j.asr.2003.02.045, 2004b.
- Cumming, A., Marcy, G. W., and Butler, R. P.: The lick planet search: detectability and mass thresholds, *Astrophys. J.*, 526, 890–915, doi:10.1086/308020, 1999.
- Hall, C. M., Dyrland, M. E., Tsutsumi, M., and Mulligan, F. J.: Temperature trends at 90 km over Svalbard, Norway ($78^\circ\text{ N } 16^\circ\text{ E}$), seen in one decade of meteor radar observations, *J. Geophys. Res.*, 117, D08104, doi:10.1029/2011JD017028, 2012.
- Horne, J. H. and Baliunas, S. L.: A prescription for period analysis of unevenly sampled time series, *Astrophys. J.*, 302, 757–763, 1986.
- Höppner, K. and Bittner, M.: Evidence for solar signals in the mesopause temperature variability?, *J. Atmos. Sol.-Terr. Phys.*, 69, 431–448, doi:10.1016/j.jastp.2006.10.007, 2007.
- Jarvis, M. J.: Planetary wave trends in the lower thermosphere – Evidence for 22-year solar modulation of the quasi 5-day wave, *J. Atmos. Sol.-Terr. Phys.*, 68, 1902–1912, doi:10.1016/j.jastp.2006.02.014, 2006.

- King, J. W.: Sun-weather relationships, *Aeronautics and Astronautics*, 13, 10–19, 1975.
- King, J. W., Hurst, E., Slater, A. J., Smith, P. A., and Tamkin, B.: Agriculture and sunspots, *Nature*, 252, 2–3, 1974.
- Lastovicka, J., Solomon, S. C., and Qian, L.: Trends in the Neutral and Ionized Upper Atmosphere, *Space Sci. Rev.*, 168, 113–145, doi:10.1007/s11214-011-9799-3, 2012.
- Lomb, N. R.: Least-squares frequency analysis of unequally spaced data, *Astrophys. Space Sci.*, 39, 447–462, 1976.
- Miyahara, H., Yokoyama, Y., and Masuda, K.: Possible link between multi-decadal climate cycles and periodic reversals of solar magnetic field, *Earth Planet. Sc. Lett.*, 272, 290–295, doi:10.1016/j.epsl.2008.04.050, 2008.
- Mokhov, I. I. and Semenov, A. I.: Nonlinear temperature changes in the atmospheric mesopause region of the atmosphere against the background of global climate changes, 1960–2012, *Dokl. Earth Sc.*, 456, 741–744, doi:10.1134/S1028334X14060270, 2014.
- Mursula, K. and Zieger, B.: Long term north-south asymmetry in solar wind speed inferred from geomagnetic activity: A new type of century-scale solar oscillation, *Geophys. Res. Lett.*, 28, 95–98, doi:10.1029/2000GL011880, 2001.
- Oberheide, J., Offermann, D., Russell III, J. M., and Mlynczak, M. G.: Intercomparison of kinetic temperature from 15 μm CO₂ limb emissions and OH*(3,1) rotational temperature in nearly coincident air masses: SABER, GRIPS, *Geophys. Res. Lett.*, 33, L14811, doi:10.1029/2006GL026439, 2006.
- Offermann, D., Donner, M., Knieling, P., and Naujokat, B.: Middle atmosphere temperature changes and the duration of summer, *J. Atmos. Sol.-Terr. Phys.*, 66, 437–450, doi:10.1016/j.jastp.2004.01.028, 2004.
- Offermann, D., Jarisch, M., Donner, M., Steinbrecht, W., and Semenov, A. I.: OH temperature re-analysis forced by recent variance increases, *J. Atmos. Sol.-Terr. Phys.*, 68, 1924–1933, doi:10.1016/j.jastp.2006.03.007, 2006.
- Offermann, D., Gusev, O., Donner, M., Forbes, J. M., Hagan, M., Mlynczak, M. G., Oberheide, J., Preusse, P., Schmidt, H., and Russel III, J. M.: Relative intensities of middle atmosphere waves, *J. Geophys. Res.*, 114, D06110, doi:10.1029/2008JD010662, 2009.
- Offermann, D., Hoffmann, P., Knieling, P., Koppmann, R., Oberheide, J., and Steinbrecht, W.: Long-term trend and solar cycle variations of mesospheric temperature and dynamics, *J. Geophys. Res.*, 115, D18127, doi:10.1029/2009JD013363, 2010.
- Offermann, D., Wintel, J., Kalicinsky, C., Knieling, P., Koppmann, R., and Steinbrecht, W.: Long-term development of short-period gravity waves in middle Europe, *J. Geophys. Res.*, 116, D00P07, doi:10.1029/2010JD015544, 2011.
- Offermann, D., Goussev, O., Kalicinsky, C., Koppmann, R., Matthes, K., Schmidt, H., Steinbrecht, W., and Wintel, J.: A case study of multi-annual temperature oscillations in the atmosphere: Middle Europe, *J. Atmos. Sol.-Terr. Phys.*, 135, 1–11, doi:10.1016/j.jastp.2015.10.003, 2015.
- Perminov, V. I., Semenov, A. I., Medvedeva, I. V., and Zheleznov, Yu. A.: Variability of mesopause temperature from hydroxyl airglow observations over mid-litudinal sites, Zvenigorod and Tory, Russia, *Adv. Space Res.*, 54, 2511–2517, doi:10.1016/j.asr.2014.01.027, 2014.
- Qu, W., Zhao, J., Huang, F., and Deng, S.: Correlation between the 22-year solar magnetic cycle and the 22-year quasicy-
cle in the Earth's atmospheric temperature, *Astron. J.*, 144, 6, doi:10.1088/0004-6256/144/1/6, 2012.
- Ryan, S. E. and Porth, L. S.: A tutorial on the piecewise regression approach applied to bedload transport data, Gen. Tech. Rep., RMRS-GTR-189, Fort Collins, CO: U.S. Department of Agriculture, Forest Service, Rocky Mountain Research Station, 2007.
- Scafetta, N. and West, B. J.: Estimated solar contribution to the global surface warming using the ACRIM TSI satellite composite, *Geophys. Res. Lett.*, 32, L18713, doi:10.1029/2005GL023849, 2005.
- Scargle, J. D.: Studies in astronomical time series analysis. II. Statistical aspects of spectral analysis of unevenly spaced data, *Astrophys. J.*, 263, 835–853, 1982.
- Scherrer, P. H., Wilcox, J. M., Svalgaard, L., Duvall Jr., T. L., Dittmeier, P. H., and Gustafson, E. K.: The mean magnetic field of the sun – Observations at Stanford, *Sol. Phys.*, 54, 353–361, 1977.
- Schmidt, C., Höppner, K., and Bittner, M.: A ground-based spectrometer equipped with an InGaAs array for routine observations of OH(3-1) rotational temperatures in the mesopause region, *J. Atmos. Sol.-Terr. Phys.*, 102, 125–139, doi:10.1016/j.jastp.2013.05.001, 2013.
- Schwarzenberg-Czerny, A.: The distribution of empirical periodograms: Lomb-Scargle and PDM spectra, *Mon. Not. R. Astron. Soc.*, 301, 831–840, doi:10.1111/j.1365-8711.1998.02086.x, 1998.
- She, C.-Y., Krueger, D. A., and Yuan, T.: Long-term midlatitude mesopause region temperature trend deduced from quarter century (1990–2014) Na lidar observations, *Ann. Geophys.*, 33, 363–369, doi:10.5194/angeo-33-363-2015, 2015.
- Svalgaard, L., Cliver, E. W., and Kamide, Y.: Sunspot cycle 24: Smallest cycle in 100 years?, *Geophys. Res. Lett.*, 32, L01104, doi:10.1029/2004GL021664, 2005.
- Thomas, S. R., Owens, M. J., and Lockwood, M.: The 22-year Hale cycle in cosmic ray flux – Evidence for direct heliospheric modulation, *Solar Phys.*, doi:10.1007/s11207-013-0341-5, 2013.
- Townsend, R. H. D.: Fast calculation of the Lomb-Scargle periodogram using graphics processing units, *Astrophys. J. Suppl. S.*, 191, 247–253, doi:10.1088/0067-0049/191/2/247, 2010.
- Wei, M., Qiao, F., and Deng, J.: A Quantitative Definition of Global Warming Hiatus and 50-Year Prediction of Global-Mean Surface Temperature, *J. Atmos. Sci.*, 72, 3281–3289, doi:10.1175/JAS-D-14-0296.1, 2015.
- White, W. B., Lean, J., Cayan, D. R., and Dettinger, M. D.: Response of global upper ocean temperature to changing solar irradiance, *J. Geophys. Res.*, 102, 3255–3266, doi:10.1029/96JC03549, 1997.
- Willet, H. C.: Recent statistical evidence in support of predictive significance of solar-climatic cycles, *Mon. Weather Rev.*, 102, 679–686, 1974.
- Zechmeister, M. and Kürster, M.: The generalised Lomb-Scargle periodogram – A new formalism for the floating-mean and Keplerian periodograms, *Astron. Astrophys.*, 496, 577–584, doi:10.1051/0004-6361/200811296, 2009.
- Zieger, B. and Mursula, K.: Annual variation in near-Earth solar wind speed: Evidence for persistent north-south asymmetry related to solar magnetic polarity, *Geophys. Res. Lett.*, 25, 841–844, doi:10.1029/98GL50414, 1998.